第 49 卷 第 9 期/2022 年 5 月/中国激光 研究论文

中国激光

基于磁致折变效应的掺铒光纤磁场传感器温度特性研究

刘思晨，黄怿*，邓传鲁，胡程勇，黄彩红，董艳华，张小贝，王廷云

上海大学特种光纤与光接入网重点实验室，上海 200444

摘要 对基于磁致折变效应的掺铒光纤磁场传感器的温度特性进行了理论分析和实验测量。理论上，基于密度泛函理论(Density Functional Theory，DFT)研究了温度对掺铒光纤磁致折变效应的影响，结果表明，温度升高会增大掺铒石英材料的原子磁矩，从而增强其磁致折变效应。实验上，基于磁致折变效应，以掺铒光纤作为 Mach-Zehnder 光纤干涉仪的传感臂，研制了磁场传感器，结果表明，干涉波谷的谐振波长随温度的升高发生红移，传感器的磁场灵敏度随之增加，16.7 ℃和 43.5 ℃温度下传感器的灵敏度分别为 12.63 pm/mT 和 25.53 pm/mT，温度变化会影响磁场的测量精度。

关键词 传感器；磁致折变效应；掺铒光纤；温度特性；磁场传感；Mach-Zehnder 干涉仪

中图分类号 TN253 **文献标志码** A **DOI**：10.3788/CJL202249.0910002

1 引 言

磁场传感器是获取磁信息的核心器件，已被广泛应用于航空导航[1]、电流检测[2]、医疗卫生[3]、交通控制[4]等领域。常见的电学磁场传感器包括原子磁力仪[5]、磁通门磁强计[6]、巨磁阻抗传感器[7]等，这些传感器普遍存在灵敏度低、动态范围小、复用性差、可靠性低等问题，难以满足磁场的实时大范围检测需求[8]。光纤磁场传感器是一种新型的光学磁场测量器件，通过检测光纤内传输光的光强[9]、相位[10]、波长[11]、偏振态[12]等参数实现磁场测量，具有体积小、成本低、耐高温、耐腐蚀、灵敏度高、响应速度快等突出优点[8,13]，并且易于复用和组网，可实现分布式传感[14]，已经成为磁场传感技术中的研究热点。

光纤磁场传感器的传感机理分为法拉第效应[15]、磁致伸缩效应[10]和磁流体[16]三类。法拉第效应使光纤中传输光的偏振面发生旋转，其旋转角度与磁场大小呈线性关系，将铽[15]、铕[17]、钬[18]等稀土元素掺杂进石英光纤可提高其 Verdet 常数，从而提升传感器的灵敏度。Sun 等[15]使用 Tb^{3+} 掺杂浓度(质量分数)为 56%的掺铽光纤研制法拉第效应型传感器，其灵敏度高达 0.49 rad/T。然而，光纤弯曲会产生线性双折射效应[19]，影响法拉第旋转角的测量精度。磁致伸缩材料如镍合金[20]、金属玻璃[21]、TbDyFe[10]等，在磁场作用下会发生形变，将此类材料涂覆在 Michelson 或 Mach-Zehnder 光纤干涉仪的传感臂上，能够使光纤中传输光的相位受到磁场调制，从而实现磁场测量。Chen 等[10]将涂覆 TbDyFe 材料的光纤作为磁场传感单元，在 200 Hz 交流磁场下获得了 69.83 mrad/μT 的传感灵敏度。然而，磁致伸缩材料大多都存在磁滞和非线性现象，不利于磁场的重复检测[22]。磁流体是一种功能型液体材料，其分子在磁场作用下会聚集成链式结构[16]，其折射率也会相应变化。将磁流体与光纤光栅[23]、微结构光纤[11]、锥形光纤[24]、Fabry-Perot 腔[25]等器件结合，可以制备高灵敏度磁场传感器。Zhao 等[25]在一个由两根单模光纤构成的 Fabry-Perot 腔内填充磁流体，实现了灵敏度高达 43.1 pm/Gs 的传感器。然而，磁流体易挥发，且受环境温度的影响大[26]，因此此类传感器的稳定性通

收稿日期：2021-08-25；**修回日期**：2021-09-28；**录用日期**：2021-10-25

基金项目：国家自然科学基金(61735009，61875116，61875118，62022053)

通信作者：*huangyi1008@shu.edu.cn

常比较差。近年来，稀土离子掺杂光纤的磁致折变效应成为研究热点。Dong 等[27]研究了铒镱共掺石英光纤的磁致折变效应，其纤芯折射率随磁场的变化率为 3.83×10^{-5} RIU/Gs($1\ \mathrm{Gs}=10^{-4}$ T，RIU 为单位折射率)，比单模光纤高 2 个数量级。直接利用掺杂光纤的磁致折变效应来实现磁场测量不失为一种良好的技术方案，可有效克服上述三类传感器的缺点。然而，环境温度是影响光纤磁致折变效应的一个重要因素，磁场传感器的温度特性具有十分重要的研究价值。

本文基于掺铒光纤的磁致折变效应，结合 Mach-Zehnder 光纤干涉仪的磁场传感技术，对传感器温度特性进行了深入研究。在理论上，基于密度泛函理论(Density Functional Theory，DFT)建立了掺铒光纤材料的微观结构模型，并计算了不同温度下该模型的结构参数和原子磁矩，研究了温度对掺铒光纤磁致折变效应的影响机理。在实验上，将 Mach-Zehnder 光纤干涉仪的传感臂掺铒光纤放入温控箱中，测量并分析了不同温度下干涉波谷的谐振波长随磁场的变化规律，研究了温度对磁场灵敏度的具体影响。磁场传感器的温度特性研究对于提高磁场测量精度具有重要的意义。

2　理论分析

根据耦合模微扰理论，光纤材料的磁光特性可通过介电张量微扰 $\Delta\boldsymbol{\varepsilon}$[28-29]来表征：

$$\boldsymbol{\varepsilon}=\begin{pmatrix}n^2&0&0\\0&n^2&0\\0&0&n^2\end{pmatrix}+\Delta\boldsymbol{\varepsilon}=\begin{pmatrix}n^2&0&0\\0&n^2&0\\0&0&n^2\end{pmatrix}+K\begin{pmatrix}0&M_z&M_y\\-M_z&0&M_x\\M_y&-M_x&0\end{pmatrix},\tag{1}$$

式中：$\boldsymbol{\varepsilon}$ 为光纤材料的介电张量；n 为与磁光效应无关的折射率；M_x、M_y 和 M_z 分别为磁化强度在坐标轴方向上的分量；$K=K'+K''$为一个与材料性质有关的复数，其中 K'与法拉第旋转的椭圆率有关，在计算中被忽略[29]，$K''=2n\theta_{\mathrm{F,sat}}/kM_{\mathrm{s}}$，$\theta_{\mathrm{F,sat}}$ 为单位距离上的饱和法拉第旋转角，k 为波数，M_{s} 为饱和磁化强度。磁场会影响光纤的磁化强度，进而改变其介电张量，最终引起光纤模式有效折射率的变化。温度会对宏观物质的磁性产生影响，宏观物质的温度特性可从物质的微观结构和原子磁矩的角度进行分析。物质的磁化强度 $\boldsymbol{M}$ 与其原子有效磁矩的关系[30]为

$$\boldsymbol{M}=\sum\boldsymbol{\mu}_{\mathrm{eff}}/V,\tag{2}$$

式中：V 为宏观物质的体积；$\boldsymbol{\mu}_{\mathrm{eff}}$ 为原子有效磁矩。磁化强度即为单位体积内所有原子有效磁矩的集合。

本文采用基于 DFT 的 Gaussian 软件分析温度对掺铒光纤磁致折变效应的影响。首先构建掺铒光纤材料的局部微观模型，以随机分散的无定型非晶硅网络结构作为石英结构模型，其中包含大量 SiO_4 四面体单元，$(SiO_4)_n$ 单元结合成环状结构(n 为硅原子数)，对应结构为 n 元环(nMR)单元[31]。为了降低计算消耗，采用 3MR 结构进行建模[32]，采用 6-31+G 基组计算石英网络结构上的氢(H)、氧(O)和硅(Si)原子的特性，采用 Stuttgart 赝势的 MWB28 基组计算铒(Er)原子的特性。掺 Er-3MR 局部微观结构模型如图 1(a)所示。采用 Multiwfn 软件计算该模型的自旋密度分布，分析 Er 原子对模型磁性的影响，如图1(b)所示。可以看出，自旋电

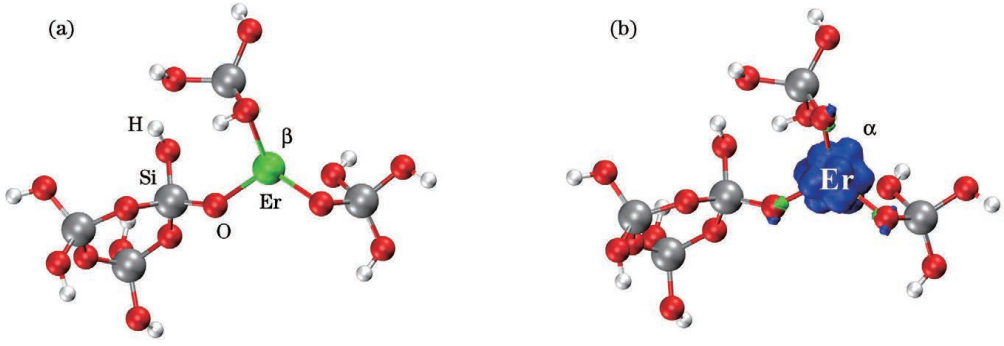

图 1　基于 DFT 的掺铒光纤材料仿真。(a)掺 Er-3MR 结构的局部微观模型；(b)自旋密度分布

Fig. 1　Simulation of erbium-doped fiber material based on DFT. (a) Local microscopic model of Er-doped-3MR structure; (b) spin density distribution

子集中在 Er 原子和 3MR 结构之间，Er 原子的 α 电子数比 O 原子的 β 电子数多，因此掺 Er-3MR 模型对外显示磁性[33]。

进一步分析温度对掺 Er-3MR 模型的结构参数和原子磁矩的影响，结果如表 1 所示。可以看出，掺 Er-3MR 模型中 Er 原子与 O 原子之间的键长（键长 1、键长 2 和键长 3）和键角（键角 1、键角 2 和键角 3）会随温度发生变化，说明掺铒光纤材料的微观结构会受到温度的影响。在 293，323，373 K 温度下，其原子磁矩分别为 2.99812μ_B、2.99826μ_B 和 2.99975μ_B，其中 μ_B 为玻尔磁子。光纤的磁致折变效应也随温度增强。

表 1　不同温度下掺 Er-3MR 模型的结构参数和原子磁矩

Table 1　Structural parameters and atomic magnetic moment of Er-doped-3MR model at different temperatures

Temperature /K	Er—O bond length /(10^{-10} m)			O—Er—O bond angle /(°)			$\lvert\boldsymbol{\mu}_{\mathrm{eff}}\rvert$ /μ_B
	1	2	3	1	2	3	
293	2.1377	2.1608	2.0863	115.7130	110.0154	117.1173	2.99812
323	2.1374	2.1606	2.0866	115.6748	109.9953	117.0797	2.99826
373	2.1372	2.1604	2.0869	116.0691	109.8899	117.0388	2.99975

本文选用的光纤是本实验室采用改进型化学气相沉积法拉制而成的掺铒光纤[34]。通过数字全息干涉系统[35]测得纤芯和包层的折射率分别约为 1.4794 和 1.4610，纤芯和包层的直径分别约为 9.87 μm 和 130.22 μm。通过扫描电子显微镜与能量色散光谱分析仪测得光纤纤芯区 Er 元素的浓度（质量分数）为 1.3 %。在 100，200，293 K 的环境温度下，采用综合物性测量系统测得掺铒光纤的磁矩，结果如图 2 所示。可以看出，在恒定磁场下，温度的升高会增大掺铒光纤的磁化强度，由式（1）可知，温度越高，其磁致折变效应越强。实验结果与前述理论分析一致。

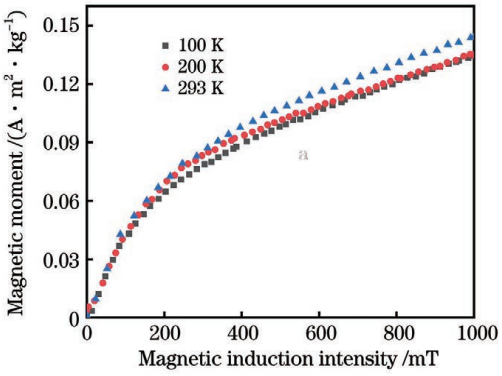

图 2　不同温度下掺铒光纤的磁矩曲线

Fig. 2　Magnetic moment curves of Er-doped fiber at different temperatures

3　磁场传感系统

图 3 为基于光纤磁致折变效应的磁场传感系统示意图。该系统主要由一个 Mach-Zehnder 光纤干涉仪构成，两段等长的光纤用作干涉仪的传感臂与参考臂，传感臂置于磁场环境中，螺线管产生的磁场方向与传感臂平行。宽带光源（Broadband Source，BBS）输出光经过耦合器 1 后被分为功率相等的两束光，分别进入传感臂和参考臂，两束光在耦合器 2 处发生干涉，干涉光强由光谱仪（Optical Spectrum Analyzer，OSA）检测。将传感臂放入温控箱中以研究温度对磁场传感的影响。

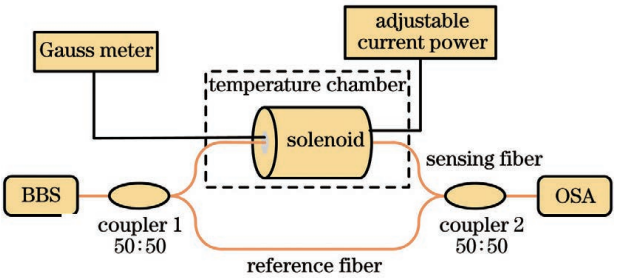

图 3　基于光纤磁致折变效应的磁场传感系统示意图

Fig. 3　Schematic of magnetic field sensing system based on magneto-refractive effect of fibers

当传感臂中传输光的基模有效折射率发生变化时，传感臂与参考臂之间将存在相位差，因此系统输出的干涉光强[36]为

$$I(\lambda)=I_1(\lambda)+I_2(\lambda)+2\sqrt{I_1(\lambda)I_2(\lambda)}\cos\left[\frac{2\pi\Delta n_{\mathrm{eff}}(B,T)L}{\lambda}\right],\quad(3)$$

式中：$I_1(\lambda)$和 $I_2(\lambda)$分别为传感臂与参考臂的输出光强；λ 为波长；L 为臂长；$\Delta n_{\mathrm{eff}}(B,T)$为传感臂与参考臂中传输光的基模有效折射率差，此参量同时受到温度和磁场的影响而发生变化，B 和 T 分别为磁感应强度和温度。当相位差满足 $\Delta\varphi=2\pi\Delta n_{\mathrm{eff}}(B,T)L/\lambda_m=(2m+1)\pi$ 时（m 为干涉级数，λ_m 为 m 级干涉波谷的谐振波长），将出现干涉波谷[37]。在恒定温度下，通过检测干涉波谷谐振波

长的漂移即可实现磁场测量。

所搭建的磁场传感系统实物图如图 4(a)所示。BBS 选用放大自发辐射(ASE)光源，干涉仪的传感臂和参考臂采用等长的掺铒光纤，其长度约为 1 m，传感光纤穿过一个螺线管中心，磁场大小被可调电流电源调控，传感臂掺铒光纤和螺线管均放入温控箱中。通过 OSA 测得波长在 1530～1560 nm 范围内的光源谱线与干涉谱，如图 4(b)所示。在实际测量中，采用高斯计实时记录磁场值，采用热电偶实时记录温度值。

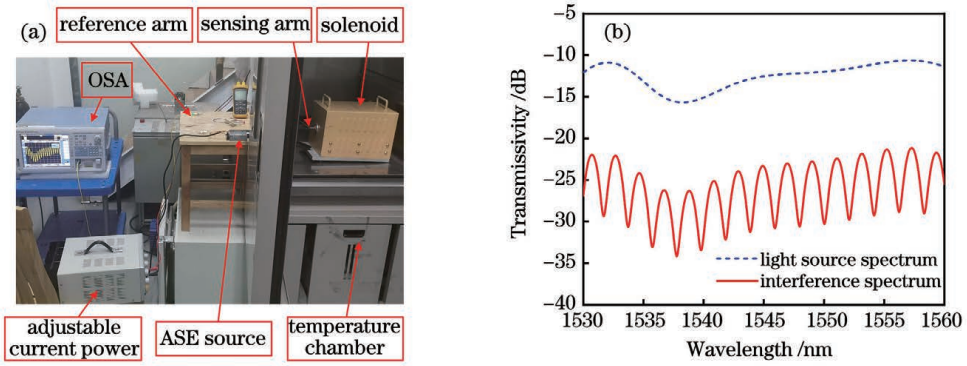

图 4　磁场传感系统的实物图与系统干涉谱测量。(a)系统实物图；(b)光源谱线与干涉谱

Fig. 4　Physical picture of magnetic field sensing system and interference spectral measurement with system. (a) Physical picture of system; (b) light source spectrum and interference spectrum

4　实验结果与讨论

4.1　传感臂光纤长度的确定

本文选用的螺线管轴向长度约为 30.4 cm，共缠绕 38 层，共计 5890 匝，最大供电电流强度约为 6 A，磁场强度最高可达 140 mT 左右。经过计算，传感光纤一次穿过螺线管的等效长度(L_{eq})为 31.638 cm[38]。

光纤正向穿过螺线管，弯曲后再反方向穿过螺线管，折返 N 次，此时掺铒光纤在螺线管内的等效长度为 NL_{eq}。当光纤等效长度为 L_{eq}、$2L_{eq}$ 和 $3L_{eq}$ 时，系统干涉谱如图 5 所示，可以看出，光纤等效长度的增加会导致系统损耗增大，且干涉谱的周期减小，干涉波峰与波谷的相对值降低。说明光纤的等效长度越长，干涉可见度越低，干涉效果越差。因此，为了获得更明显的干涉谱，本文选择等效长度为 L_{eq} 的掺铒光纤进行磁场测量。

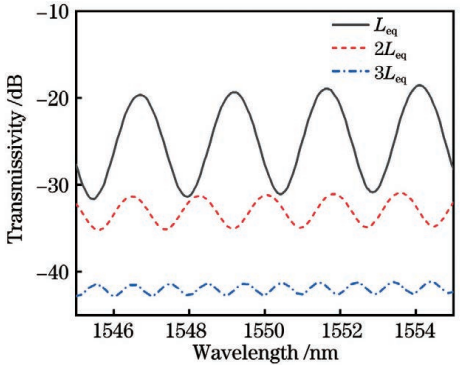

图 5　不同光纤等效长度下的系统干涉谱

Fig. 5　Interference spectra of system with different equivalent fiber lengths

图 6(a)给出了在 0～93.7 mT 磁场范围内系统干涉谱的变化规律，环境温度为 16.7 ℃。随着磁场

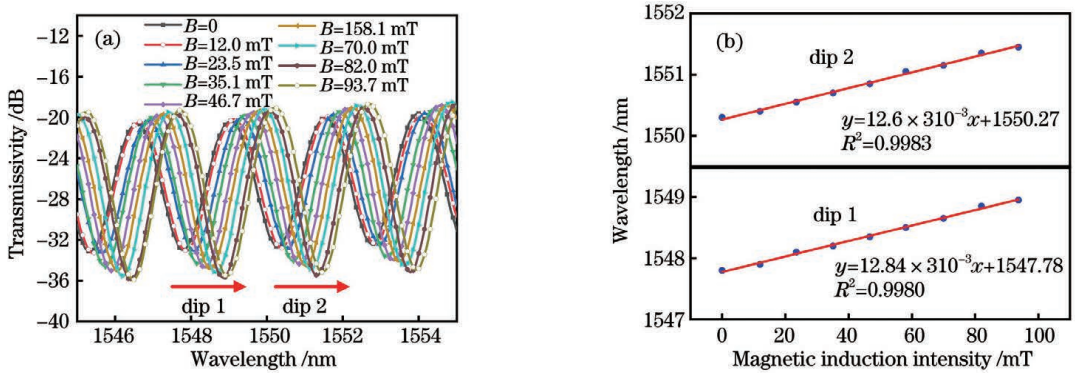

图 6　磁场传感实验结果。(a)不同磁场作用下的干涉谱；(b)谐振波长与磁感应强度的关系

Fig. 6　Experimental results of magnetic field sensing. (a) Interference spectra under different magnetic fields; (b) resonance wavelength versus magnetic induction intensity

的增加，1548 nm 和 1550 nm 附近的干涉波谷 dip 1 和 dip 2 的谐振波长发生了红移。图 6(b)进一步给出了 dip 1 和 dip 2 的谐振波长与磁场强度的关系，通过线性拟合可得，谐振波长对磁场的响应灵敏度分别为 12.84 pm/mT 和 12.63 pm/mT，线性度(R^2)分别为 0.9980 和 0.9983。

4.2　温度对磁场传感的影响

调节温控箱内的温度，并采用热电偶同时记录螺线管的温度和环境温度，当两者温度相同时，记录当前磁场下的干涉谱，此测量方式可确保螺线管温度与环境温度一致。图 7(a)～(c)分别给出了 0，46.7，93.7 mT 磁场作用下系统干涉谱随温度的变化规律，可以看出，当磁场恒定时，干涉波谷的谐振波长随温度的升高而发生红移。测得不同温度下 1550 nm 附近干涉波谷 dip 2 的谐振波长与磁场强度的关系，如图 7(d)所示，在 16.7，26.1，34.3，43.5 ℃温度下，磁场灵敏度分别为 12.63，17.26，21.18，25.53 pm/mT，线性度分别为 0.9980、0.9981、0.9964 和 0.9970。

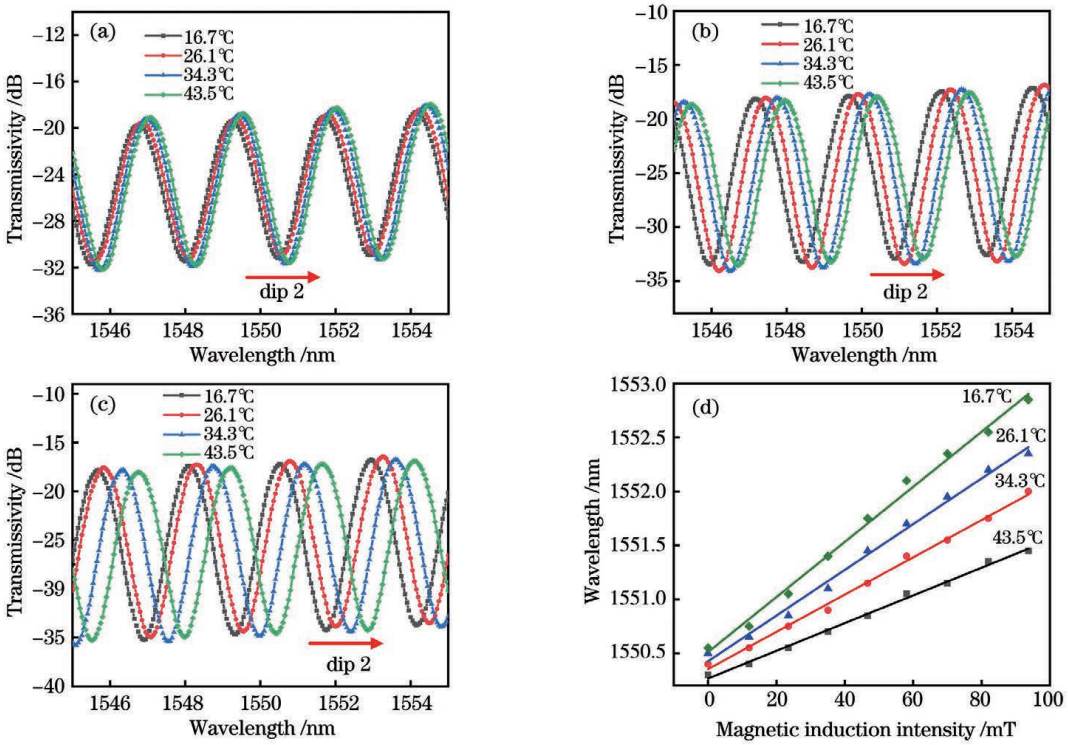

图 7　温度对磁场传感的影响。(a)0，(b)46.7 mT，(c)93.7 mT 磁场作用下，干涉波谷随温度的变化；(d)不同温度下谐振波长与磁感应强度的关系

Fig. 7　Effect of temperature on magnetic field sensing. Change of interference valley with temperature under (a) 0, (b) 46.7 mT, and (c) 93.7 mT magnetic fields; (d) resonance wavelength versus magnetic induction intensity at different temperatures

总之，传感器的磁场灵敏度会随温度的升高而增加，其原因在于，温度升高会增大掺铒光纤材料的原子磁矩，进而增强光纤的磁致折变效应，最终影响测量结果。因此，在实际应用中，需要对其进行温度补偿，以提高磁场测量精度。本文获得的磁场传感灵敏度与基于光纤光栅[23]、Fabry-Perot 腔[25]或微谐振腔[39]的传感器相比略低，但灵敏度皆在同一数量级，如表 2 所示。然而，本文的磁场传感方案利用光纤本体的磁致折变效应，无需借助磁感应材料如磁流体，不仅简化了传感结构，还克服了磁流体易挥发而导致的传感器稳定性差的缺点。

表 2　不同光纤磁场传感器的性能比较

Table 2　Performance comparison of various optical-fiber magnetic field sensors

Sensor type	Magnetic field sensitivity / [pm·(mT)$^{-1}$]
Fiber grating[23]	81.0
Fabry-Perot cavity[25]	43.1
Micro-resonator[39]	37.3
Proposed sensor	12.63

后续工作将从以下两方面进行优化：一是采用 Bragg 光栅等器件作为温度传感器对磁场传感器进

行修正，实现温度补偿[40]；二是研制磁光效应强且受温度影响较小的材料如 As_2S_3[41]等掺杂光纤。

5 结 论

基于掺铒光纤的磁致折变效应，结合 Mach-Zehnder 光纤干涉仪的磁场传感技术，研究了温度对传感器磁场传感性能的影响。在理论上，基于 DFT 理论，建立了掺铒光纤材料的微观结构模型，并对该模型在不同温度下的结构参数及原子磁矩进行了仿真计算。结果表明，随着温度的增加，Er—O 键长、O—Er—O 键角发生变化，原子磁矩单调增大，从而增强了磁致折变效应。在实验上，以掺铒光纤作为传感臂，研制了 Mach-Zehnder 光纤干涉型磁场传感器。结果表明，磁场灵敏度随温度的升高而增大，16.7 ℃和 43.5 ℃温度下其灵敏度分别为 12.63 pm/mT 和 25.53 pm/mT。基于掺铒光纤磁致折变效应的磁场传感器温度特性研究对推动该传感器的实用化具有十分重要的意义。

参 考 文 献

[1] Lenz J, Edelstein S. Magnetic sensors and their applications[J]. IEEE Sensors Journal, 2006, 6(3): 631-649.

[2] Huang Y H, Xia L, Pang F B, et al. Self-compensative fiber optic current sensor[J]. Journal of Lightwave Technology, 2021, 39(7): 2187-2193.

[3] Saran D, Sagar R, Gaur M S. Study of human blood under influence of magnetic field by AC dielectric and thermally stimulated discharge current methods[J]. Journal of Thermal Analysis and Calorimetry, 2019, 136(4): 1679-1686.

[4] Lenz J E. A review of magnetic sensors[J]. Proceedings of the IEEE, 1990, 78(6): 973-989.

[5] 杨宝，缪培贤，史彦超，等. 二能级磁共振经典物理图像的理论和实验研究[J]. 中国激光，2020，47(10)：1012001.
Yang B, Miao P X, Shi Y C, et al. Theoretical and experimental studies on classic physical picture of two-level magnetic resonance[J]. Chinese Journal of Lasers, 2020, 47(10): 1012001.

[6] 丁鸿佳，隋厚堂. 磁通门磁力仪和探头研制的最新进展[J]. 地球物理学进展，2004，19(4)：743-745.
Ding H J, Sui H T. The recent progress of the Fluxgate Magnetometer and sensor[J]. Progress in Geophysics, 2004, 19(4): 743-745.

[7] Vacher F, Alves F, Gilles-Pascaud C. Eddy current nondestructive testing with giant magneto-impedance sensor[J]. NDT & E International, 2007, 40(6): 439-442.

[8] 张军英. 新型光纤磁场传感技术研究[D]. 西安：西北大学，2019：6-11.
Zhang J Y. Study on novel fiber-optic magnetic sensors[D]. Xi'an: Northwest University, 2019: 6-11.

[9] Shi F, Bai X K, Wang F, et al. All-fiber magnetic field sensor based on hollow optical fiber and magnetic fluid[J]. IEEE Sensors Journal, 2017, 17(3): 619-622.

[10] Chen F F, Jiang Y, Jiang L. 3×3 coupler based interferometric magnetic field sensor using a TbDyFe rod[J]. Applied Optics, 2015, 54(8): 2085-2090.

[11] 李佳欢，裴丽，王建帅，等. 基于光子晶体光纤表面等离子体共振的温度和磁场双参量传感器[J]. 中国激光，2019，46(2)：0210002.
Li J H, Pei L, Wang J S, et al. Temperature and magnetic field sensor based on photonic crystal fiber and surface plasmon resonance[J]. Chinese Journal of Lasers, 2019, 46(2): 0210002.

[12] Ma R D, Wan L X, Liu X H, et al. Polarization in D-shaped fiber modulated by magneto-optical dichroism of magnetic fluid[J]. Chinese Optics Letters, 2020, 18(1): 010601.

[13] 李敏，尹辑文. 基于磁性聚合物薄膜的光纤磁场传感探针[J]. 中国激光，2019，46(11)：1106002.
Li M, Yin J W. Fiber magnetic field sensing probe based on magnetic polymer thin film[J]. Chinese Journal of Lasers, 2019, 46(11): 1106002.

[14] Mizuno Y, Theodosiou A, Kalli K, et al. Distributed polymer optical fiber sensors: a review and outlook[J]. Photonics Research, 2021, 9(9): 1719-1733.

[15] Sun L, Jiang S, Marciante J R. All-fiber optical magnetic-field sensor based on Faraday rotation in highly terbium-doped fiber[J]. Optics Express, 2010, 18(6): 5407-5412.

[16] 李永倩，温芳芳，王劭龙. 基于磁流体的温度磁场测量技术研究进展[J]. 激光与光电子学进展，2021，59(5)：0500003.
Li Y Q, Wen F F, Wang S L. Research progress of temperature and magnetic field dual-parameter measurement technology based on magnetic fluid[J]. Laser & Optoelectronics Progress, 2021, 59(5): 0500003.

[17] Huang Y, Chen H C, Dong W L, et al. Fabrication of europium-doped silica optical fiber with high Verdet constant[J]. Optics Express, 2016, 24(16): 18709-18717.

[18] Liu Z M, Chen Z Y, Chen N, et al. Study of the Verdet constant of the holmium-doped silica fiber[J]. OSA Continuum, 2020, 3(5): 1096-1104.

[19] Perciante C D, Aparicio S, Illa R, et al. Nonplanar fiber-optic sensing head for the compensation of bending-induced birefringence in Faraday current sensors[J]. Applied Optics, 2015, 54(18): 5708-5714.

[20] Hu Q B, An X Y, Chen L F, et al. High-magnetic-field solidification on magnetostrictive effect of Ni-doped MnCoSi alloy[J]. Materials Letters, 2021, 301: 130268.

[21] Grishin A M, Ignakhin V S, Lugovskaya L A, et al. Crystallization kinetics and magnetostriction properties of amorphous $Fe_{80-x}Co_xP_{14}B_6$ metallic glasses[J]. Journal of Magnetism and Magnetic Materials, 2020, 512: 166972.

[22] 段沐森, 李鹏, 刘盛春. 光纤磁场传感器[J]. 黑龙江大学自然科学学报, 2020, 37(4): 477-483.
Duan M S, Li P, Liu S C. Fiber-optic magnetic field sensor[J]. Journal of Natural Science of Heilongjiang University, 2020, 37(4): 477-483.

[23] Gao R, Lu D F, Zhang Q, et al. Temperature compensated three-dimension fiber optic vector magnetic field sensor based on an elliptical core micro fiber Bragg grating[J]. Optics Express, 2020, 28(5): 7721-7733.

[24] 汪成程, 范荣华, 吴根柱, 等. 基于磁流包覆冷却拉锥全光纤磁场传感器特性研究[J]. 激光与光电子学进展, 2020, 57(1): 010602.
Wang C C, Fan R H, Wu G Z, et al. Characteristics of all-optical-fiber magnetic field sensor based on magnetic fluid coating and cooling tapering[J]. Laser & Optoelectronics Progress, 2020, 57(1): 010602.

[25] Lü R Q, Zhao Y, Wang D, et al. Magnetic fluid-filled optical fiber Fabry-Pérot sensor for magnetic field measurement[J]. IEEE Photonics Technology Letters, 2014, 26(3): 217-219.

[26] Chen Y F, Yang S Y, Tse W S, et al. Thermal effect on the field-dependent refractive index of the magnetic fluid film[J]. Applied Physics Letters, 2003, 82(20): 3481-3483.

[27] Dong Y H, Huang C H, Sun W T, et al. Magneto-refractive effect and mechanism analysis of erbium-ytterbium co-doped silica fiber[J]. IEEE Photonics Journal, 2021, 13(3): 1-11.

[28] Dötsch H, Bahlmann N, Zhuromskyy O, et al. Applications of magneto-optical waveguides in integrated optics: review[J]. Journal of the Optical Society of America B, 2005, 22(1): 240-253.

[29] Pintus P. Accurate vectorial finite element mode solver for magneto-optic and anisotropic waveguides[J]. Optics Express, 2014, 22(13): 15737-15756.

[30] 刘龙. 稀土基磁性多层膜中的磁相互作用和磁畴结构[D]. 合肥: 中国科学技术大学, 2021: 2-5.
Liu L. Magnetic interaction and domain structures in rare-earth-based magnetic multilayers[D]. Hefei: University of Science and Technology of China, 2021: 2-5.

[31] Wen J X, Wang T Y, Pang F F, et al. Photoluminescence characteristics of $Bi^{(m+)}$-doped silica optical fiber: structural model and theoretical analysis[J]. Japanese Journal of Applied Physics, 2013, 52(12R): 122501.

[32] Sitarz M, Mozgawa W, Handke M. Rings in the structure of silicate glasses[J]. Journal of Molecular Structure, 1999, 511/512: 281-285.

[33] Wehrmann C M, Imran M, Pointer C, et al. Spin multiplicity effects in doublet versus singlet emission: the photophysical consequences of a single electron[J]. Chemical Science, 2020, 11(37): 10212-10219.

[34] Wang Q, Wen J X, Luo Y H, et al. Enhancement of lifetime in Er-doped silica optical fiber by doping Yb ions via atomic layer deposition[J]. Optical Materials Express, 2020, 10(2): 397-407.

[35] 谷婷婷, 黄素娟, 闫成, 等. 基于数字全息图的光纤折射率测量研究[J]. 物理学报, 2015, 64(6): 064204.
Gu T T, Huang S J, Yan C, et al. Refractive index measurement research for optical fiber based on digital hologram[J]. Acta Physica Sinica, 2015, 64(6): 064204.

[36] 贾振安, 段维维, 刘颖刚, 等. 波长和强度同时响应的锥形多模光纤温度传感器[J]. 应用光学, 2017, 38(2): 0208001.
Jia Z A, Duan W W, Liu Y G, et al. Tapered multi-mode fiber temperature sensor based on simultaneous response of wavelength and intensity[J]. Journal of Applied Optics, 2017, 38(2): 0208001.

[37] Layeghi A, Latifi H, Frazão O. Magnetic field sensor based on nonadiabatic tapered optical fiber with magnetic fluid[J]. IEEE Photonics Technology Letters, 2014, 26(19): 1904-1907.

[38] 王华军, 李宏福, 温越琼. 螺线管中磁场的计算[J]. 四川轻化工学院学报, 1999, 12(4): 23-25.
Wang H J, Li H F, Wen Y Q. Magnetic field calculate in solenoid[J]. Journal of Sichuan Institute of Light Industry and Chemical Technology, 1999, 12(4): 23-25.

[39] Mahmood A, Kavungal V, Ahmed S S, et al. Magnetic field sensing using whispering-gallery modes in a cylindrical microresonator infiltrated with ferronematic liquid crystal[J]. Optics Express, 2017, 25(11): 12195-12202.

[40] Zhao Y, Lü R Q, Wang D, et al. Fiber optic Fabry-Perot magnetic field sensor with temperature compensation using a fiber Bragg grating[J]. IEEE Transactions on Instrumentation and Measurement, 2014, 63(9): 2210-2214.

[41] Sato H, Kawase M, Saito M. Temperature dependence of the Faraday effect in As-S glass fiber [J]. Applied Optics, 1985, 24(15): 2300-2303.

Temperature Characteristics of Er-Doped Fiber Magnetic Field Sensor Based on Magneto-Refractive Effect

Liu Sichen, Huang Yi*, Deng Chuanlu, Hu Chengyong, Huang Caihong, Dong Yanhua, Zhang Xiaobei, Wang Tingyun

Key Laboratory of Specialty Fiber Optics and Optical Access Networks, Shanghai University, Shanghai 200444, *China*

Abstract

Objective Optical-fiber magnetic field sensors have advantages such as small size, light weight, high temperature resistance, corrosion resistance, and high sensitivity, which can realize distributed sensing and long-distance signal transmission. Its technology has been a popular research issue in magnetic field sensing area. Optical-fiber magnetic field sensors can be approximately classified into three types: Faraday effect, magnetostrictive effect, and magnetic fluid. However, fiber bending may cause the linear birefringence effect, which influences the measurement accuracy of the sensors based on Faraday effect. The sensors based on the magnetostrictive effect is not suitable for repeated detection owing to the hysteresis and nonlinear effect, which happens to the most magnetostrictive materials. The stability of the sensors based on magnetic fluid is low owing to the volatileness and the temperature sensitivity of magnetic fluid. In recent years, the magneto-refractive effect of rare-earth-doped fibers has been a popular research issue. It is an effective technical solution to use the magneto-refractive effect of fibers for magnetic field sensing, which can overcome the disadvantages of the above sensors. However, the ambient temperature influences the magneto-refractive effect of fibers, which may affect the measurement accuracy. Therefore, there is significant value to studying the temperature characteristics of magnetic field sensors based on the magneto-refractive effect of fibers.

Methods The magneto-refractive effect of Er-doped fiber is analyzed by Gaussian software based on the density functional theory (DFT). Considering the computing resources, 3-membered-rings (3MR) is used to build the microstructure model for Er-doped materials. 6-31 + G basis is used to calculate oxygen, hydrogen, and silicon elements. The Stuttgart pseudo-potential MWB28 basis is used to calculate the erbium element in the model. The structural parameters and atomic magnetic moments of the Er-doped-3MR model at different temperatures are calculated for studying the relationship between the magneto-refractive effect of the Er-doped fiber and temperature. The magnetic field sensing system is mainly composed of an optical-fiber Mach-Zehnder interferometer. Two Er-doped fibers with the same length are used as the sensing arm and the reference arm. The sensing arm fiber is placed in a solenoid, which can generate a magnetic field parallel to the fiber axis. The output light of the broadband source is divided into two beams with equal power after passing through the coupler 1, and enters the sensing arm and the reference arm, respectively. Two beams interfere at the coupler 2 and the interference light is detected by an optical spectral analyzer. At a constant temperature, the magnetic field measurement is performed by detecting the interference spectral shift with the magnetic field. The sensing arm fiber and solenoid are placed in a temperature chamber for studying the influence of temperature on magnetic field sensing.

Results and Discussions With the increase of temperature, the structural parameters of the Er-doped-3MR model change, and the atomic magnetic moment increases, which indicates that the increase of temperature enhances the magneto-refractive effect of the Er-doped fiber. With the increase of the equivalent length of the sensing arm fiber, the loss of the magnetic field sensing system increases, the period of the interference spectrum decreases, and the relative intensity of interference peak and trough decreases (Fig. 5), which indicates that the longer the equivalent length of the fiber, the lower the interference visibility and the worse the interference effect. Therefore, to obtain

an obvious interference spectrum, an Er-doped fiber with a length of L_{eq} is chosen for the magnetic field measurement. At 16.7 ℃, the interference troughs near 1548 nm and 1550 nm perform a red-shift when the magnetic field increases from 0 to 93.7 mT. The response sensitivities of the resonance wavelengths of the troughs to the magnetic field are 12.84 pm/mT and 12.63 pm/mT, respectively (Fig. 6). The temperature chamber is used to adjust the ambient temperature. When the magnetic field is constant, the interference trough near 1550 nm performs a red-shift with the increase of temperature. The sensitivity to magnetic field is 12.63, 17.26, 21.18 and 25.53 pm/mT at 16.7, 26.1, 34.3 and 43.5 ℃, respectively (Fig. 7). The magnetic field sensitivity increases as the temperature increases, which is owing to the enhancement of the magneto-refractive effect of the Er-doped fiber at the sensing arm. Thus, the temperature compensation is required to improve the measurement accuracy. The sensor can be optimized in the following aspects. First, the devices such as Bragg gratings are used as temperature sensors to modify the magnetic field sensor. Second, the novel fibers with a strong magneto-optic effect and a low temperature sensitivity, such as As_2S_3-doped fibers, are fabricated.

Conclusions The influence of temperature on the magnetic field sensor based on the magneto-refractive effect of an Er-doped fiber and an optical-fiber Mach-Zehnder interferometer is studied in this paper. In theory, the microstructure model of the Er-doped fiber material is established based on DFT. The structural parameters and atomic magnetic moments of the model are calculated at different temperatures. The numerical results indicate that as the temperature increases, the Er—O bond length and O—Er—O bond angle change, and the atomic magnetic moment increases monotonously, enhancing the magneto-refractive effect of the fiber. In experiment, an Er-doped fiber is used as the sensing arm of an optical-fiber Mach-Zehnder interferometer to fabricate the magnetic field sensor. The experimental results indicate that the magnetic field sensitivity increases with the increase of temperature. The sensitivities of the sensor to magnetic field are 12.63 pm/mT at 16.7 ℃ and 25.53 pm/mT at 43.5 ℃, respectively. The study on temperature characteristics of the magnetic field sensor is helpful to improve the accuracy of the sensor, and is of great significance to its practical application.

Key words sensors; magneto-refractive effect; Er-doped fiber; temperature characteristic; magnetic field sensing; Mach-Zehnder interferometer